

Visual-stimuli Four-arm Maze test to Assess Cognition and Vision in Mice

Jean-Philippe Vit¹, Dieu-Trang Fuchs¹, Ariel Angel², Aharon Levy²,
Itschak Lamensdorf², Keith L. Black¹, Yosef Koronyo¹ and Maya Koronyo-Hamaoui^{1, 3, *}

¹Department of Neurosurgery, Maxine Dunitz Neurosurgical Research Institute, Cedars-Sinai Medical Center, Los Angeles, CA, 90048, USA

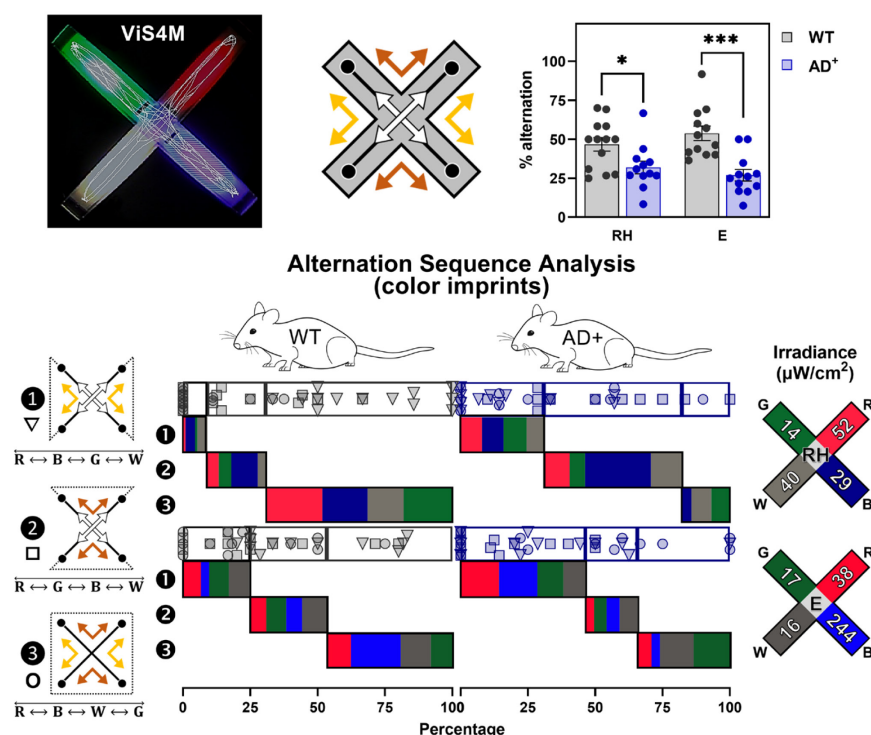
²Pharmaseed Ltd., Ness Ziona 74047, Israel

³Department of Biomedical Sciences, Division of Applied Cell Biology and Physiology, Cedars-Sinai Medical Center, Los Angeles, CA, USA

*For correspondence: maya.koronyo@csmc.edu

[Abstract] Visual impairments, notably loss of contrast sensitivity and color vision, were documented in Alzheimer's disease (AD) patients yet are critically understudied. This protocol describes a novel visual-stimuli four-arm maze (ViS4M; also called visual x-maze), which is a versatile x-shaped maze equipped with spectrum- and intensity-controlled light-emitting diode (LED) sources and dynamic grayscale objects. The ViS4M is designed to allow the assessment of color and contrast vision along with locomotor and cognitive functions in mice. In the color testing mode, the spectral distributions of the LED lights create four homogenous spaces that differ in chromaticity and luminance, corresponding to the mouse visual system. In the contrast sensitivity test, the four grayscale objects are placed in the middle of each arm, contrasting against the black walls and the white floors of the maze. Upon entering the maze, healthy wild-type (WT) mice tend to spontaneously alternate between arms, even under equiluminant conditions of illumination, suggesting that cognitively and visually intact mice use both color and brightness as cues to navigate the maze. Evaluation of the double-transgenic APP_{SWE}/PS1_{ΔE9} mouse model of AD (AD⁺ mice) reveals substantial deficits to alternate in both color and contrast modes at an early age, when hippocampal-based memory and learning is still intact. Profiling of timespan, entries, and transition patterns between the different arms uncovers variable aging and AD-associated impairments in color discrimination and contrast sensitivity. The analysis of arm sequences of alternation reveals different pathways of exploration in young WT, old WT, and AD⁺ mice, which can be used as color and contrast imprints of functionally intact versus impaired mice. Overall, we describe the utility of a novel visual x-maze test to identify behavioral changes in mice related to cognition, as well as color and contrast vision, with high precision and reproducibility.

Graphic abstract:



Exploratory behavior of AD⁺ mice versus age- and sex-matched WT mice is tracked (top left: trajectory from a 5-min video file) in a novel visual-stimuli four-arm maze (ViS4M; also named visual x-maze) equipped with spectrum- and intensity-controlled LED sources or grayscale objects.

Consecutive arm entries reveal that APP_{SWE}/PS1_{ΔE9} (AD⁺) mice alternate less between arms, as opposed to WT mice. Sequence analysis, according to the three alternation pathways (depicted by white, yellow, and brown arrows) under different conditions of illumination, uncovers specific deficits linked to color vision in AD⁺ mice, evidenced by a color imprint chart.

Keywords: Rodent maze, Cognition, Visual impairments, Behavioral changes, Neurodegenerative disease, Aging, Apparatus, Retinal pathology

[Background] Mounting evidence indicates that the pathology of Alzheimer’s Disease (AD) is not restricted to the brain but also extends to the retina. Multiple studies have shown that the retina of mild cognitively impaired (MCI) and AD patients exhibit the neuropathological hallmarks of AD – amyloid β-protein (Aβ) plaques and hyperphosphorylated tau – along with gliosis, vascular dysfunctions, and neuronal degeneration (Blanks *et al.*, 1996a and 1996b; Koronyo-Hamaoui *et al.*, 2011; La Morgia *et al.*, 2016; Koronyo *et al.*, 2017; Dumitrascu *et al.*, 2020; Lee *et al.*, 2020; Lemmens *et al.*, 2020; Shi *et al.*, 2020b; Dumitrascu *et al.*, 2021; Shi *et al.*, 2021; Ngolab *et al.*, 2021; Tadokoro *et al.*, 2021). Moreover, retinal pathology appears to mirror the disease in the brain (Koronyo-Hamaoui *et al.*, 2011; La Morgia

et al., 2016; Koronyo *et al.*, 2017; Doustar *et al.*, 2020, Dumitrascu *et al.*, 2020; Shi *et al.*, 2020a and 2020b; Risacher *et al.*, 2020). Clinically, both color and contrast sensitivity were significantly impaired in AD patients when compared with healthy individuals (Chang *et al.*, 2014; Polo *et al.*, 2017). Indeed, visual impairments are among the earliest symptoms documented in these patients, especially loss of contrast sensitivity (Crow *et al.*, 2003; Risacher *et al.*, 2013; Javaid *et al.*, 2016; Salobar-García *et al.*, 2019) and altered color vision reminiscent of tritanomaly, an abnormality of blue-sensitive retinal cones (Cronin-Golomb *et al.*, 1993; Wijk *et al.*, 1999; Salobar-García *et al.*, 2019).

Sporadic and transgenic animal models of AD recapitulate AD pathology in the retina and present A β deposits and tauopathy that are linked with inflammation, vasculopathy, and neurodegeneration (Perez *et al.*, 2009; Koronyo-Hamaoui *et al.*, 2011; Koronyo *et al.*, 2012; Hart *et al.*, 2016; Doustar *et al.*, 2017; Grimaldi *et al.*, 2018; Hampel *et al.*, 2018; Georgevsky *et al.*, 2019; Chibhabha *et al.*, 2020, Doustar *et al.*, 2020; Habiba *et al.*, 2020; Shi *et al.*, 2020a; Shi *et al.*, 2021). Transgenic mouse models of AD also show disturbances in the visual system, reduced function of ganglion cells and photoreceptors, as well as reduction of inner retinal thickness and atrophy of the visual cortex (Crisuolo *et al.*, 2018; Chiquita *et al.*, 2019). However, the specific visual changes in color and contrast vision have not been previously examined in transgenic mouse models of AD.

Behavioral assessment of color vision and contrast sensitivity in C57BL/6 mice has been previously conducted by optomotor response (Sinex *et al.*, 1979; Prusky *et al.*, 2004), optokinetic reflex (van Alphen *et al.*, 2009), and forced-choice procedures. The latter includes the visual water task (Jacobs *et al.*, 2004; Prusky and Douglas, 2004), psychometric curves in freely moving mice (Busse *et al.*, 2011), and the visual-stimulation environment (Denman *et al.*, 2018). Forced-choice paradigms require days of training and thousands of trials, which are less suitable for aged mice, especially for sensitive, high-attrition rate AD-model mice.

We created the behavioral visual-stimuli four-arm maze (ViS4M or visual x-maze), a novel, controlled, and user-friendly behavioral apparatus specialized for the detection of vision changes in mice (Vit *et al.*, 2021). Unlike previous behavioral tests, the ViS4M is highly sensitive and reproducible, allowing mice to move freely without introducing stress. Importantly, the test relies entirely on innate exploratory behavior and does not require a pre-training phase nor rewards. Moreover, this test can simultaneously assess locomotor, cognitive, and visual functions. We investigated color and contrast sensitivity in the double-transgenic APP_{SWE}/PS1 Δ E9 (AD⁺) mice. These AD-model mice and wild-type (WT) mice were tested at three different ages, during six sessions (5 min each) of testing, in five color modes (five conditions of illumination), and one contrast mode. Using the novel ViS4M, we identified early and progressive impairments in color vision and contrast sensitivity in AD-model mice.

In the present manuscript, we provide a detailed description and step-by-step configuration of the ViS4M and accessories, with numerous notes and tips in the equipment and procedure sections. In the data analysis section, we review all the parameters analyzed in the original study (total entries, timespan, alternation, and transitions) with their calculations and supported by relevant examples. We also present an additional analysis of alternation arm sequences and make freely available our own ViS4M Toolbox V1, which includes two Excel spreadsheets to automatically calculate all the aforementioned parameters

upon inputting a sequence of arm entries in color and contrast modes. The comprehensive analysis of alternation sequences, as well as unidirectional and bidirectional transitions in combination with linear regressions and visualization tools, allow a better understanding of the locomotor, cognitive, and visual functions of mice measured in the ViS4M.

Materials and Reagents

Animals

1. Double transgenic B6.Cg-Tg(APP_{SWE}/PSEN1_{ΔE9})85Dbo/Mmjax hemizygous (AD⁺) mouse strain [RRID:MMRRC_034832-JAX], initially purchased from the Mutant Mouse Resource and Research Center (MMRRC) at the Jackson Laboratory, then bred and maintained at Cedars-Sinai Medical Center.

2. Non-transgenic wild-type (WT) littermates (Jackson Laboratory, catalog number: 000664)

The mouse colony is housed in a humidity- and temperature-controlled (21-22°C) vivarium on a 12:12-h light/dark cycle (lights on at 8:00 am; lights off at 8:00 pm) with free access to food and water.

Three different cohorts of mice are tested, each representing a different age: 8.5-month-old WT (n=13; 9 males and 4 females) and AD⁺ (n=12; 9 males and 3 females), 13-month-old WT (n=11; 6 males and 5 females) and AD⁺ (n=11; 4 males and 7 females), and 18-month-old WT (n=19; 11 males and 8 females) and AD⁺ (n = 9; 5 males and 4 females).

Note: The double-transgenic APP_{SWE}/PS1_{ΔE9} is a well-established mouse strain, with early-onset pathology of AD in the hippocampus and cortex (β-amyloid plaques, severe astrogliosis, and microgliosis, as well as brain plasticity deficits and synaptic loss). We and others also reported AD manifestation in the retina of these mice (Ning et al., 2008; Koronyo et al., 2012; Mirzaei et al., 2019; Doustar et al., 2020, Shi et al., 2020a and 2020b). Importantly, cognitive deficits in these mice have been well documented and reproducible. We developed the ViS4M to further characterize visual function, especially color vision and contrast sensitivity. AD pathology in the retina of other mouse strains has been confirmed, such as the aggressive-phenotype 5xFAD or the triple-transgenic 3xTg mice (Criscuolo et al., 2018; Grimaldi et al., 2018; Habiba et al., 2020). This protocol could be implemented on different AD mouse strains, normal aging, and other neurodegenerative models to evaluate visual function.

Equipment

- A. Visual-stimuli four-arm maze (ViS4M) apparatus

Note: The visual-stimuli four-arm maze (ViS4M or Visual X-maze) that we describe below was conceived and developed in-house by our team. The prototype used to collect the present data shares the same specifications (including the color LED lights) with the now commercially available ViS4M manufactured by Maze Engineers (<https://conductscience.com/maze/portfolio/visual-x-maze>

[vis4m/](#)).

1. Backbone of apparatus

- a. Custom-made x-shaped enclosure built with 15 cm-high black plexiglass walls attached to a glass base

Each arm is perpendicular to the two adjacent arms and is 45 cm long and 10 cm wide (Figure 1A-1B).

- b. Removable transparent floor plates that can be installed at two different levels (6 cm or 11 cm above the glass base) in each arm and in the center of the ViS4M (Figure 1C)

- c. White translucent acrylic plates that can be inserted below each floor level by sliding within small track brackets made of plexiglass (Figure 1C-1D)

Note: Behavioral testing is carried out either on the upper level (color mode) or the lower level (contrast mode) but not simultaneously on both levels.

- d. The center of the apparatus is a neutral area with no white translucent plate and no light source directly below it (Figure 1A-1C)

- e. Plastic transparent covers with perforated holes to help with breathing

Note: Color vision and contrast sensitivity are different aspects of vision that involve different photoreceptors. While the contrast mode involves the function of rods (lower mesopic range), the color mode requires functional cones (transition between mesopic and photopic range). These two modalities of testing are complementary to appreciate the functionality of rod and cone photoreceptors.

2. Light-emitting diode (LED) lights (for color mode)

Each LED strip source consists of an array of surface-mounted device (SMD) 3528 LED chips evenly spaced in four rows (27 LED chips per row) and is individually inserted in each arm of the ViS4M, directly onto the glass base (Figure 1D). Spectra of the light sources were determined using an Ocean Optics USB2000 spectrometer and further validated with a Sekonic C700-U spectrometer (Figure 1E).

- a. Red monochromatic light: wavelength (λ) = 628 nm, full width at half maximum (FWHM) = 17 nm

- b. Green monochromatic light: λ = 517 nm, FWHM = 31 nm

- c. Blue monochromatic light: λ = 452 nm, FWHM = 22 nm

- d. White light: λ_1 = 441 nm, FWHM = 19 nm and λ_2 = 533 nm, FWHM = 104 nm

The white LED is made of a blue-emitting diode that also excites a yellow-emitting phosphor [cerium doped yttrium aluminum garnet (Ce:YAG-Y3Al5O12) crystals] embedded in the epoxy dome.

Note: The criterion for choosing the LED colors is as follows: the red light as a dark-space control arm with low- to no-color stimulus; the green light to stimulate the mouse retinal M-opsin in M-cones, without stimulating S-opsin; and the blue light to stimulate the mouse retinal S-opsin in S- and M-cones, in addition to the M-opsin.

The following components control the brightness of the light stimuli.

- e. LED single color dimmers using pulse width modulation (PWM) technology
- f. Individual remote devices to control the dimmers

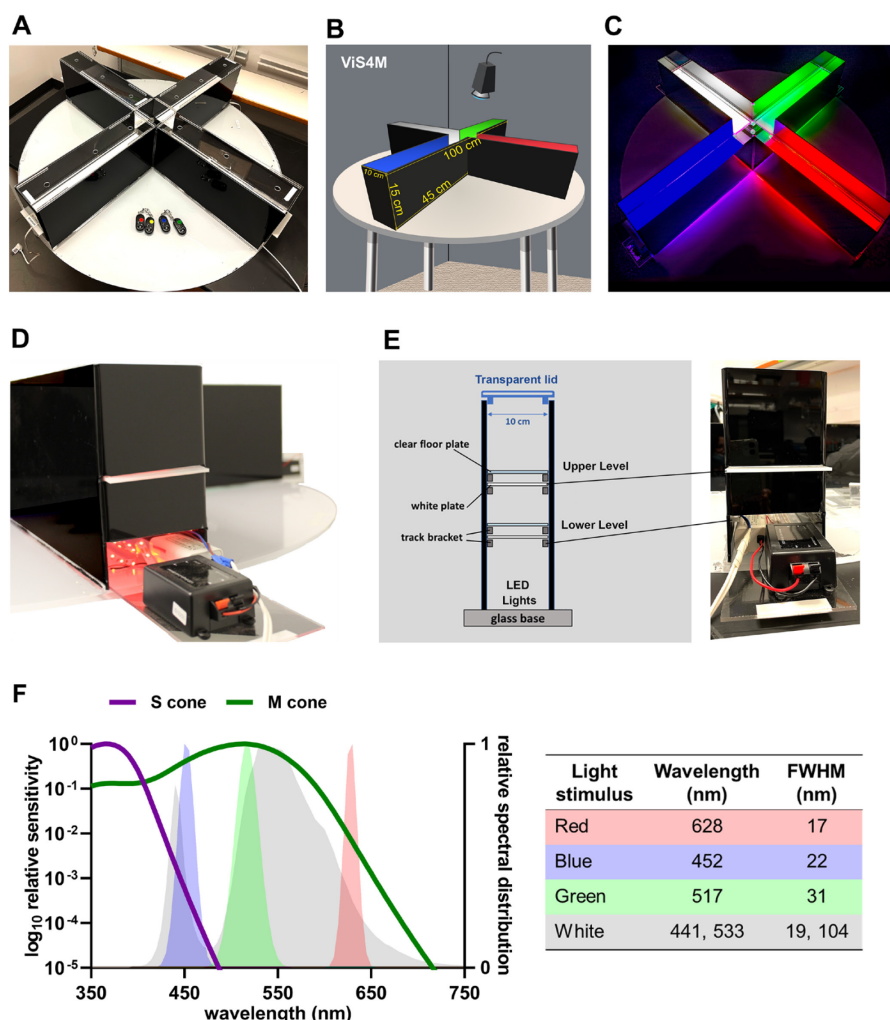


Figure 1. Characteristics of the ViS4M in color mode.

(A) Photograph and (B) illustration of the x-shaped ViS4M in color mode with apparatus measurements. (C) Photograph of the ViS4M in color mode, E condition, showing the illuminated arms. (D) Photograph of an arm with the opening for the red lights and with the white translucent plate inserted at the upper level. (E) Illustration of the positioning of the clear floor and white translucent diffuser plates within the arms of the maze, paired with a photograph of the outside front-view of an arm. (F) Spectral distribution of the LED sources according to mouse M- and S-opsins sensitivity with table showing the characteristics of the light stimuli (wavelength, FWHM).

3. Grayscale objects (for contrast mode)

Four objects have the following characteristics (Figure 2A).

- a. Identical shape of a right-angled triangular prism
- b. Dimensions: base (adjacent side) = 5 cm; height (opposite side) = 1 cm
- c. Different shades (black, gray, white, and clear) that create different contrasts with the black walls and white floors of the maze (Figure 2B)

The luminance ratios of the objects against the black walls and/or white floors as measured with a light meter are indicated below.

- d. Black object against the black walls = 1.06 (minimal to no contrast)
- e. Gray object against the black walls = 6.00
- f. White object against the black walls = 9.69 (high contrast against the black walls but minimal contrast with the white floor)
- g. Clear object against the black walls = 6.56
- h. Flexible positioning and location for the placement of the grayscale objects to accommodate investigator's goals

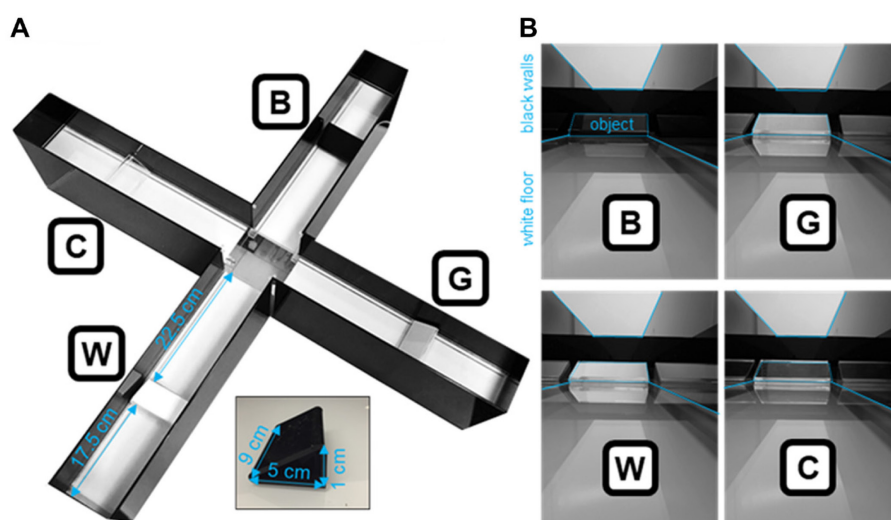


Figure 2. Characteristics of the ViS4M in contrast mode.

(A) Photograph of the ViS4M in contrast mode with measurements for positioning of the grayscale objects. (B) Photographs of the objects within each arm as seen from the center of the ViS4M. Objects, black walls, and white floors are delineated to better assess contrasts. (A-B) B, Black; C, Clear; G, Gray; W, White.

B. Other accessories

1. Sekonic Flashmate L-308S light meter (Sekonic, catalog number: 401-309)
2. Timer
3. Digital USB camera

Note: A color camera is preferable to identify the colored arms. However, a black and white camera can be used, provided the position of each arm on the screen is recorded. A short clip of the apparatus positioning can be made prior to each testing session with the lights of the room turned on and the arms identified by name.

4. USB camera varifocal lens with 2.8-12 mm focal length

Software

1. Rodent Toolbox V1 (freely available at <https://www.ndcn.ox.ac.uk/team/stuart-peirson>)
2. ANY-maze behavior tracking software 6.3 (www.stoeltingco.com/anymaze/video-tracking/software.html) or other video tracking software, such as EthoVision XT (www.noldus.com/ethovision-xt)
3. ViS4M Toolbox V1 (Supplementary file: [ViS4M Toolbox V1](#))
4. GraphPad Prism 9.0
5. ParallelSets V2 (freely available at [Parallel Sets \(eagereyes.org\)](http://Parallel Sets (eagereyes.org)))
6. Circos online (freely available at mkweb.bcgsc.ca/tableviewer/)

Procedure

A. Configuration of the ViS4M

1. Place the transparent floor inside the arms at the chosen level and insert the center zone transparent floor at the same level (color mode: upper level; contrast mode: lower level) (Figure 1C).
2. Position the clear plastic covers on top of the arms.
3. Slide the translucent white plates within the brackets below the floors (Figure 1D).
4. Set up the visual stimuli.
 - a. Color mode only: Install the LED light sources directly on top of the glass base in their respective arm (Figure 1D).

Note: The arrangement of the LED chips in combination with the white translucent plates and the clear covers is optimized to allow the light to diffuse equally in all directions and create a spatially homogenous stimulus. No individual LED spots are discernable.
 - b. Contrast mode only: position the grayscale objects individually, in the middle of their respective arm, on their base, with their opposite side facing at $\frac{1}{2}$ -length (22.5 cm) of the entrance of the arm (Figure 2A-2B).

B. Configuration of the light intensities according to the illumination conditions

1. Plug the light sources into a power outlet.
2. Turn on the lights using the individual remote controls, then turn off the ambient light of the room. The following steps pertain to the use of a Sekonic Flashmate L-308S light meter to measure incident illuminance (page 19 of operating manual).
3. Attach the Lumidisc accessory to the light meter.
4. Set EV (Exposure Value) mode and ISO 100 on the device.
5. Position the flat surface of the light meter sensor facing and about 2 cm above the floor (mouse eye level) at a locus situated in the middle of the arm.

Note: The positioning of the sensor and locus of measurement were chosen for consistency and

practicability, assuming the light coming from each LED source diffused in all directions equally into its respective arm.

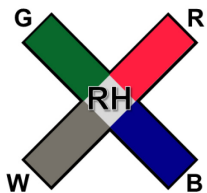
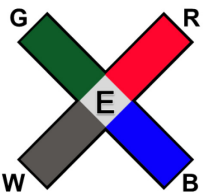
6. Take the measurement.
7. Adjust the brightness of the light stimulus using the remote control and take a new measurement, if necessary.
8. Record the EV and proceed to the other three arms following steps 5 through 7.
9. Convert the recorded EV to illuminance units (lux) and luminance units (cd/m^2) using the relationships $\text{lux} = 2.5 \times 2^{\text{EV}}$ and $\text{cd/m}^2 = 2^{(\text{EV}-3)}$, respectively.

Note: Illuminance and luminance are photometric measures of perceived brightness of a light source as it relates to the human eye according to the spectral sensitivity function. Although they provide informative characteristics of the light source to the human experimenter, they are irrelevant to the mouse visual system. Radiometric measures of irradiance should be used and can be estimated using the Rodent Toolbox V1 (freely available at <https://www.ndcn.ox.ac.uk/team/stuart-peirson>).

10. In the Rodent Toolbox V1 (under Toolbox tab), select the type of light source.
11. Enter the details (λ , FWHM) and illuminance (lux) of the light stimulus.
12. Record the estimated irradiance ($\mu\text{W/cm}^2$).

Note: In our original Scientific Reports manuscript (Vit et al., 2021), we describe five different conditions of illumination. For the purpose of this protocol, we provide data analysis from two out of these five configurations: Red High (RH) and Equal (E) conditions. Photometric and radiometric characteristics of these two conditions are shown in Table 1.

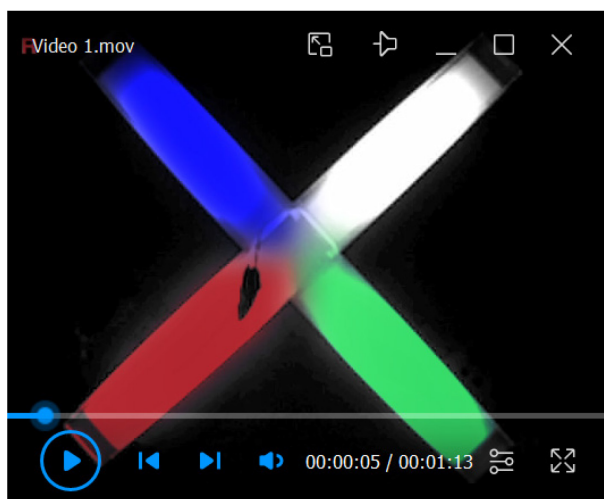
Table 1. Photometric and radiometric measures and estimations of the light stimuli

	Red High				Equal			
								
	R	B	G	W	R	B	G	W
EV	5.4	1.9	4.7	6.0	4.9	4.9	4.9	4.7
Illuminance (lux)	103	9	66	164	76	75	73	67
Luminance (cd/m^2)	4.4	0.4	3.2	8.1	3.7	3.6	3.7	3.3
Irradiance ($\mu\text{W/cm}^2$)	52	29	14	40	38	244	17	16

From the measurements of EV (using the Sekonic L-308S light meter) to the calculation of estimated photometric (illuminance, luminance) and radiometric characteristics (irradiance) of the four light sources under RH and E conditions of illumination

C. Configure the camera for video recording

1. Position the camera with the varifocal lens above the ViS4M.
2. Connect the camera to a laptop via USB port and open ANY-maze behavior tracking software.
Note: We do not track animal trajectory in real time. However, we use ANY-maze behavior tracking software to record and save video files of all testing sessions for later analysis. A free version of the software can be used for this purpose.
3. Use the varifocal lens so the entire apparatus fits the image.
4. Adjust the exposure to obtain acceptable contrast of the mouse over the background for tracking
Note: A small portion at the end of the arms is significantly darker upon illumination as compared to the middle of the arms. To set the exposure, we use small black objects (remote controls) across the arms to verify contrast is sufficient in the entire apparatus.
5. Re-adjust the exposure in between each condition of illumination.



Video 1. A video of a mouse exploring the ViS4M in the color mode.

The sequence of colored arm entries and alternations are indicated (speed $\times 2$).

D. Behavioral testing (Video 1)

1. Turn off the ambient light of the room.
2. (Contrast mode only) Turn on dim red-light illumination (mesopic, ~ 0.1 cd/m²).
Note: All testing takes place in the dark during the last third of the light cycle (between 4:00 pm and 8:00 pm). The sole light source is provided by the illuminated arms of the ViS4M. Mice are only tested once a day. Different conditions of testing (in color and contrast mode) are carried out on consecutive days.
3. Bring the mice to the testing room.
4. Leave the animals undisturbed for a short 30-min period of time to habituate to the dark room.
5. At the end of the acclimation period, proceed with the testing of the first mouse.
Note: We recommend tail-marking mice the day prior to testing for easy and fast identification. Since the lights of the testing room are turned off, a flashlight can be used if necessary.

6. Start the video recording and present the mouse ID to the camera.
7. Identify the mouse in its home cage and place it in the center of the maze through the opened top.
8. Cover the opened center of the apparatus with a clear plastic or Plexiglass plate and start the timer.
9. Leave the mouse to freely explore the maze for 5 min.

Note: We recommend counting the number of entries during testing. A minimum of eight entries is required to assure an appropriate number of four-arm alternations (see Data analysis for definition of parameters). In contrast mode, the presence of the objects does not prevent the mice from fully exploring the arms of the ViS4M. Most of the mice show no hesitation to jump over the objects to reach the distal part of the arms.

10. After 5 min, return the mouse to its home cage and pause the video recording.
11. Wipe the floors and walls with a solution of 70% isopropyl alcohol, then thoroughly wipe any excess of alcohol with a dry cloth.
Note: By the time the next mouse is placed in the apparatus following this procedure (~3 min, steps 6-7), any residual trace of alcohol will have evaporated.
12. Proceed with the next mouse following steps 6 through 10.

Data analysis

The data generated from behavioral testing in the ViS4M cover several behavioral domains. A list of parameters, behaviors, and analysis tools is shown in Table 2.

Table 2. List of analyzed parameters

Parameter	Behavior	Analysis tool
Distance traveled	Locomotion, general activity	ANY-maze
Average speed	Locomotion, general activity	ANY-maze
Total number of entries	Locomotion, general activity	ViS4M Toolbox V1
% spontaneous alternation	Cognition, color/contrast discrimination	ViS4M Toolbox V1
% time in each colored arm	Color/contrast preference	ANY-maze
% entries in each colored arm	Color/contrast preference	ViS4M Toolbox V1
% unidirectional transitions	Color/contrast discrimination	ViS4M Toolbox V1
% bidirectional transitions	Color/contrast discrimination	ViS4M Toolbox V1

We created the [ViS4M Toolbox V1](#), two Excel spreadsheets made available freely with this protocol. Upon entering the sequence of arm entries recorded from video files (see Video 1), the ViS4M Toolbox V1 calculates the total number of entries, the percentage of spontaneous alternation, the percentage of entries in each colored arm, as well as the percentages of unidirectional and bidirectional transitions between arms.

All the cells in the spreadsheet that pertain to the identification of the study, the mice, and the condition

of testing (columns A through F) are unlocked and can be filled according to the user's experiment.

The text sequence of arm entries is entered in column G in lower case. The keys differ in the two spreadsheets: 'r' for 'red,' 'b' for 'blue,' 'g' for 'green,' 'w' for 'white' in the color toolbox, and 'c' for 'clear,' 'b' for 'black,' 'g' for 'gray,' 'w' for 'white' in the contrast toolbox. All the cells with calculated parameters are locked to prevent the inclusion of errors.

Additional information specific to these parameters and their calculation in the ViS4M Toolbox V1 is detailed below as well as in Table 3.

Note: Alternatively, the user can choose to calculate these parameters directly in a video tracking software. However, the use of definitions other than those described below will lead to discrepancies with the data generated in the ViS4M Toolbox V1.

Table 3. Description of parameters and calculations

Parameters	wrbwgrgrwrbgrwbggrgwbr	n	Calculation
characters (x)	xxxxxxxxxxxxxxxxxxxxxxx	21	
entries (e)	_eeeeeeeeeeeeeeeeeeee	$e = x - 1$	20
4-arm sequences (s)	---sssssssssssssssss	$s = e - 2$	18
	-rbwg --bwgr -----wrbg -----bgrw -----grwb -----rwbg -----wbgr -----rgwb -----gwbr		
alternation (a)		9	$\% a = (a \times 100) \div (e - 2)$ 50%
red entries (r)	-r---r-r-r---r---r	7	$\% r = (r \times 100) \div e$ 35%
blue entries (b)	--b-----b---b---b-	4	$\% b = (b \times 100) \div e$ 20%
green entries (g)	---g-g---g---g-g---	5	$\% g = (g \times 100) \div e$ 25%
white entries (w)	_--w---w---w---w--	4	$\% w = (w \times 100) \div e$ 20%
2-arm transitions (t)	-ttttttttttttttttttt	$t = e$	20
red-to-blue ($r \rightarrow b$)	-rb-----rb-----	2	$\% r \rightarrow b = (r \rightarrow b \times 100) \div t$ 10%
blue-to-red ($b \rightarrow r$)	-----b-r	1	$\% b \rightarrow r = (b \rightarrow r \times 100) \div t$ 5%
bidirectional ($r \leftrightarrow b$)		3	$\% r \leftrightarrow b = \% r \rightarrow b + \% b \rightarrow r$ 15%

red-to-green ($r \rightarrow g$)	-----rg-----rg----	2	$\% r \rightarrow g = (r \rightarrow g \times 100) \div t$	10%
green-to-red ($g \rightarrow r$)	-----grgr-----gr--gr----	4	$\% g \rightarrow r = (g \rightarrow r \times 100) \div t$	20%
bidirectional ($r \leftrightarrow g$)		6	$\% r \leftrightarrow g = \% r \rightarrow g + \% g \rightarrow r$	30%
red-to-white ($r \rightarrow w$)	-----rw-----rw-----	2	$\% r \rightarrow w = (r \rightarrow w \times 100) \div t$	10%
white-to-red ($w \rightarrow r$)	wr-----wr-----	2	$\% w \rightarrow r = (w \rightarrow r \times 100) \div t$	10%
bidirectional ($r \leftrightarrow w$)		4	$\% r \leftrightarrow w = \% r \rightarrow w + \% w \rightarrow r$	20%
blue-to-green ($b \rightarrow g$)	-----bg--bg-----	2	$\% b \rightarrow g = (b \rightarrow g \times 100) \div t$	10%
green-to-blue ($g \rightarrow b$)	-----	0	$\% g \rightarrow b = (g \rightarrow b \times 100) \div t$	0%
bidirectional ($b \leftrightarrow g$)		2	$\% b \leftrightarrow g = \% b \rightarrow g + \% g \rightarrow b$	10%
blue-to-white ($b \rightarrow w$)	--bw-----	1	$\% b \rightarrow w = (b \rightarrow w \times 100) \div t$	5%
white-to-blue ($w \rightarrow b$)	-----wb--wb-	2	$\% w \rightarrow b = (w \rightarrow b \times 100) \div t$	10%
bidirectional ($b \leftrightarrow w$)		3	$\% b \leftrightarrow w = \% b \rightarrow w + \% w \rightarrow b$	15%
green-to-white ($g \rightarrow w$)	-----gw--	1	$\% g \rightarrow w = (g \rightarrow w \times 100) \div t$	5%
white-to-green ($w \rightarrow g$)	--wg-----	1	$\% w \rightarrow g = (w \rightarrow g \times 100) \div t$	5%
bidirectional ($g \leftrightarrow w$)		2	$\% g \leftrightarrow w = \% g \rightarrow w + \% w \rightarrow g$	10%

From a text sequence to entries, alternation, and transitions: example entered in the ViS4M Toolbox V1.

A. Total entries

Instrumental to obtaining an accurate arm sequence is the definition of arm entry. We implement the following rules when recording arm entries:

1. In general, while exploring the maze, mice enter an arm, then walk within the arm until they reach the other end (dead-end), turn around, exit the arm, and visit another arm (see Video 1). In this case, this is straightforward, and we count an entry as the entire body of the mouse (tail not included) crossing the virtual border between the squared center and the open end of the arm.
2. There are occurrences when mice enter the arm as described above but do not reach the end of the arm (see Video 1). Whether these events should be counted as entries is difficult to generalize to the entire population or a specific group of mice. We include these entries or not after careful review of video files. For consistency, we do not make our choice at the entry level; thus, for a particular mouse, we either count all or do not count any of this type of entry.
3. Two or more consecutive entries in the same arm are counted as one entry. (Alternatively: account re-entries as multiple entries but ensure consistency within the same experiment.)

Note: There are several reasons why we counted consecutive entries in the same arm as a single entry. First, they are infrequent events (5%). Second, to our knowledge, it is customary to analyze revisiting the same arm as a single entry with similar mazes, such as the Y-maze. Third, it would not alter the sequence of exploration in terms of color or contrast cues. Lastly,

accounting for them considerably complicates the combinations for successful and unsuccessful alternations, requires analyzing 5-arm sequences (for example, the sequences 'brgw' and 'brrgw' are both successful alternations between the 4 colors), and consequently increases the possibility of calculation errors.

4. The first entry of the sequence is not counted. Indeed, when the mouse is released in the center of the maze at the beginning of the test, it often runs inside the arm it is facing, and this is not considered a deliberate choice.

Note: Although the first arm in the sequence is not counted as an entry, it is taken into consideration for the first alternation and first transition.

The total number of entries can be used as an indicator of locomotor activity since it predicts with high fidelity the distance traveled ($R^2 = 0.8275$, $P < 0001$) and the average speed ($R^2 = 0.8317$, $P < 0001$) of the animal estimated with the tracking software ANY-maze (Figure 3A). The coefficient factor of 1.1 between entries and distance corresponds to twice the sum of the lengths of an arm and the center of the maze $[(0.45\text{ m} + 0.10\text{ m}) \times 2 = 1.1\text{ m}]$.

Note: The distance traveled and the average speed are two basic features of most tracking software; consequently, their estimation using ANY-maze is not described in the present protocol.

B. Alternation

Perhaps the main feature of the ViS4M is its capability to assess both cognition and visual function. Spontaneous alternation is defined as the consecutive visits of the four different arms without returning to an arm already visited in a four-arm sequence (see Video 1). In standard three-arm models such as the Y-maze or the T-maze, the percentage of spontaneous alternation (number of alternations out of total number of three-arm sequences during the testing session) represents spatial navigation and working memory (Kraeuter *et al.*, 2019).

The following are characteristics of four-arm sequences and alternations in the four-arm ViS4M (see also Table 3).

1. The first four-arm sequence is counted at the third arm entry, and each subsequent entry adds a new four-arm sequence.
2. From a specific starting arm, there are 6 alternation sequences out of 27 four-arm sequence possibilities (total in the entire apparatus: 24 alternations out of 108 possible sequences). Thus, the chance to perform an alternation in a four-arm sequence is $\frac{2}{9}$ or about 22%.

When introduced to a uniformly configured ViS4M (NS, no stimulus), WT mice alternate about 10% above chance (Figure 3B). However, when the four arms are set with predefined light modalities or grayscale objects, the percentage of alternation is significantly increased to about 50% as compared to NS (Stimulus, $F_{(2.599, 38.98)} = 5.007$, $P = 0.0069$) in these same mice (Figure 3B). This result suggests that cognitively and visually intact mice use the visual stimuli of the ViS4M as cues to navigate the maze, and are consequently able to discriminate between some or all of the arms, based on differences in chromaticity, brightness, and/or contrast.

AD⁺ mice are largely inept to alternate as early as 8.5 months up to 18 months of age when compared to WT littermates (Figure 3C) in color mode, under RH (Genotype, $F_{(1, 69)} = 35.31$, $P < 0.0001$) and E conditions (Genotype, $F_{(1, 67)} = 38.14$, $P < 0.0001$), and in contrast mode (Genotype, $F_{(1, 71)} = 57.90$, $P < 0.0001$), suggesting visual and/or cognitive deficits (see discussion in Vit *et al.*, 2021). There is no significant difference in alternations between males and females within each genotype at any age in RH, E, and CT conditions (Figure 3D). However, in color mode, while the impairment appears earlier in male (8.5 months) than in female (13-18 months) AD⁺ mice compared to gender-matched WT mice (Figure 3D), the progression with age is more noticeable in female AD⁺ mice, with a dramatic decline in alternation between 8.5 and 18 months, especially under E condition (Age, $F_{(2, 26)} = 4.312$, $P = 0.0241$). In contrast mode, early deficits appear in both male and female AD⁺ mice (Figure 3D). Between 8.5 and 18.5 months, decline in contrast sensitivity is most apparent in WT mice (Genotype \times Age, $F_{(2, 71)} = 3.869$, $P = 0.0254$), independently of gender (Figure 3C-3D).

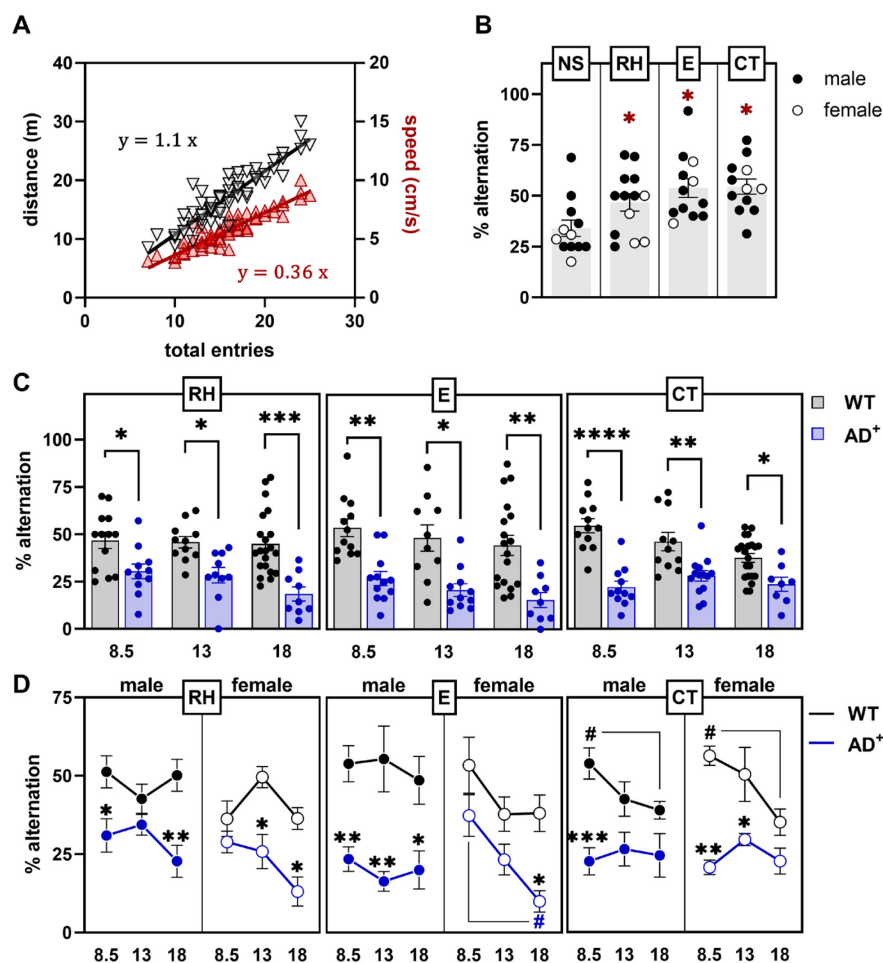


Figure 3. Spontaneous alternation with and without color illumination.

(A) Linear regression of the total number of arm entries during a 5-min testing session, with the distance traveled in the ViS4M and the average speed of mice. (B) Percentages of alternation in the ViS4M without stimuli (NS, no stimulus), with color illumination (RH, red high; E, equal), or

with grey-scale objects (CT, contrast) of young adult (8.5 months) WT mice. □ $P < 0.05$, NS versus RH, E, CT modes. (C) Percentages of alternation in 8.5-, 13-, and 18-month-old WT and AD⁺ mice under RH, E, and CT conditions. □ $P < 0.05$, □ □ $P < 0.01$, □ □ □ $P < 0.001$, □ □ □ □ $P < 0.0001$, WT versus AD⁺ mice. (D) Percentages of alternation in 8.5-, 13-, and 18-month-old male and female WT and AD⁺ mice under RH, E, and CT condition. □ $P < 0.05$, □ □ $P < 0.01$, gender-matched WT versus AD⁺ mice; # (WT) or # (AD⁺) $P < 0.05$, 8.5 versus 18 months.

Additional characteristics of alternation are listed below.

- The sequences of alternations can be categorized into three pathways as shown in Table 4 and as illustrated in Figure 4A-4B.
- In each pathway, alternation sequences can start at each of the four arms and in two directions, leading to eight combinations (Figure 4C). The lack or the abundance of an alternation sequence starting at a specific arm can indicate the position of discontinuities within a pathway of alternation.
- In the ViS4M, the paths are: □ $\overleftrightarrow{R} \leftrightarrow B \leftrightarrow G \leftrightarrow W$, □ $\overleftrightarrow{R} \leftrightarrow G \leftrightarrow B \leftrightarrow W$, and □ $\overleftrightarrow{R} \leftrightarrow B \leftrightarrow W \leftrightarrow G$ (Table 4 and Figure 4B).

Table 4. Classification of pathways of alternation and four-arm sequences

Parameters	wrbwgrgrwrbgrwbgwbr	n	Calculation
entries (<i>e</i>)	_____		20
4-arm sequences (<i>s</i>)	----ssssssssssssssss	$s = e - 2$	18
4-arm alternation (<i>a</i> ₄)	-rbwg --bwgr -----wrbg -----bgrw -----grwb -----rwbg -----wbgr -----rgwb -----gwbr	9	$\% a_4 = (a_4 \times 100) \div (e - 2)$ 50%
path □ $\overleftrightarrow{r} \leftrightarrow b \leftrightarrow g \leftrightarrow w$	-----wrbg	1	$\% \textcircled{1} = (\textcircled{1} \times 100) \div a_4$ 12%
path □ $\overleftrightarrow{r} \leftrightarrow g \leftrightarrow b \leftrightarrow w$	-----bgrw -----grwb -----rwbg -----wbgr	4	$\% \textcircled{2} = (\textcircled{2} \times 100) \div a_4$ 44%

path \square $r \leftrightarrow b \leftrightarrow w \leftrightarrow g$	-rbwg --bwgr -----rgwb -----gwbr	4	% $a_4 = (a_4 \times 100) \div a_4$	44%
3-arm alternation (a_3)	wrbw -----rbgr	2	% $a_3 = (a_3 \times 100) \div (e - 2)$	11%
2/3-arm alternation ($a_{2/3}$)	---wgrg -----rgrw -----grwr -----rwrb -----bgrg -----grgw	6	% $a_{2/3} = (a_{2/3} \times 100) \div (e - 2)$	33%
2-arm alternation (a_2)	----grgr	1	% $a_2 = (a_2 \times 100) \div (e - 2)$	6%

Categories (4-arm, 3-arm, 2/3-arm, and 2-arm alternations) and subcategories (pathways \square , \square , and \square of alternation): same example as in Table 3.

The detailed analysis of alternation sequences of 8.5-month-old WT and AD⁺ mice under the RH condition is presented in Figures 4B and 4C. The stacked bar graph with individual data points [Path \square (○), Path \square (□), Path \square (▽)] in Figure 4B shows that WT mice more frequently alternate in path \square , as opposed to paths \square and \square , while AD⁺ mice alternate mostly in paths \square and \square (Genotype \times Path, $F_{(2, 44)} = 14.50$, $P < 0.0001$). Within path \square , AD⁺ mice are not or rarely capable of completing an alternation when starting from the red or the blue arm as opposed to WT mice (Genotype, $F_{(1, 22)} = 30.34$, $P < 0.0001$).

We use parallel sets charts to visualize sequences of alternation. Figure 4C illustrates the alternation pathway \square of WT and AD⁺ mice under RH condition. WT mice (green ribbons) show eight ribbons of equal proportion, corresponding to the eight possible alternations in this pathway. AD⁺ mice (purple ribbons) only exhibit limited sequences of alternations, suggesting deficient discrimination between colored arms. Overall, these data point out an incapacity of AD⁺ mice to visit the green, white, and blue arms successively, suggesting difficulties in discriminating between these three arms.

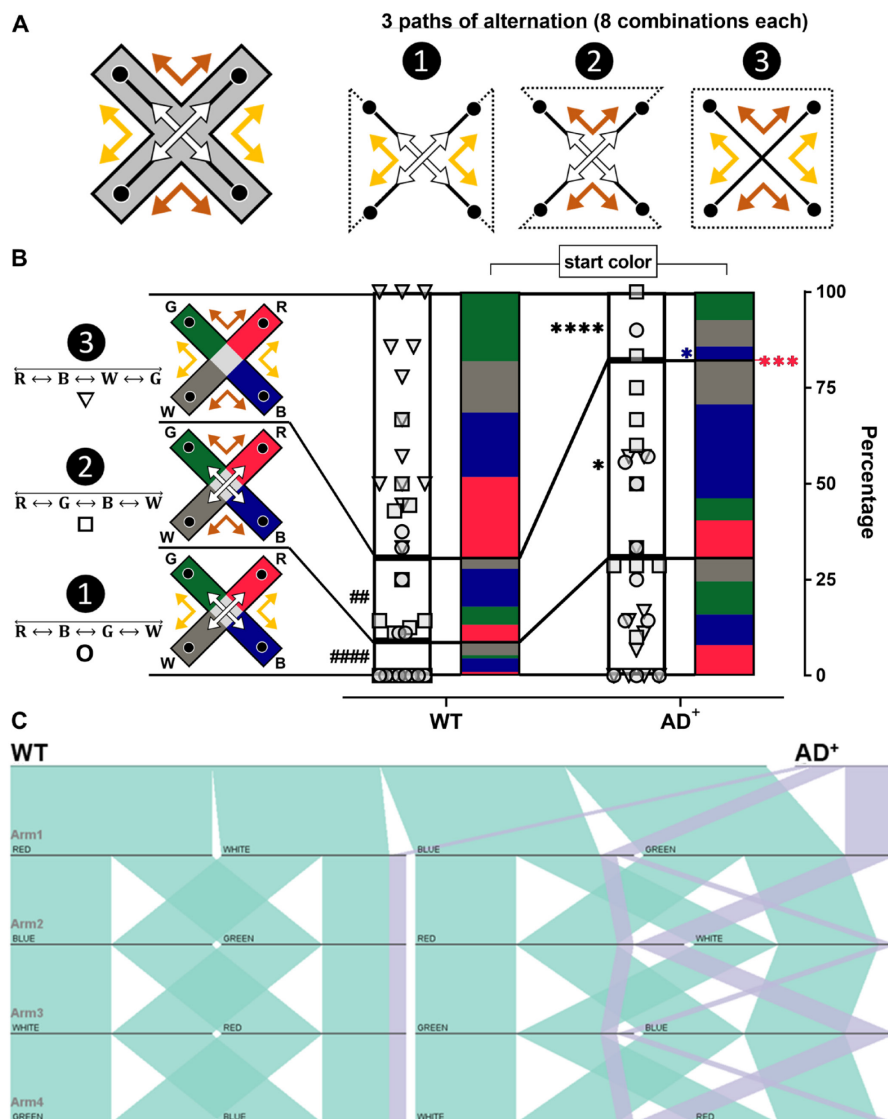


Figure 4. Arm sequence analysis of alternations in the color mode test.

(A) Illustration of the 3 pathways of alternation in the Vis4M. (B) Proportions of the three pathways and their starting arm in 8.5-month-old WT and AD⁺ mice under RH condition. Alternation sequence pathways are shown as stacked bars with individual data points. Path □ (○), Path □ (□), Path □ (▽). ### $P < 0.01$, #### $P < 0.0001$, WT mice, Paths □ and □ versus Path □; □ $P < 0.05$, □ □ □ □ $P < 0.0001$, Paths □ and □, WT versus AD⁺ mice; □ □ □ $P < 0.001$, Path □, red arm start, WT versus AD⁺ mice; □ $P < 0.05$, Path □, blue arm start, WT versus AD⁺ mice. (C) Visualization of alternation sequences in 8.5-month-old WT (green ribbons) and AD⁺ mice (purple ribbons) under RH condition (Path □: R ↔ B ↔ W ↔ G) using parallel sets chart.

Since alternations only account for approximately 50% and 20% of all four-arm sequences in WT and AD⁺ mice, respectively, we further analyze 4-arm sequences. In addition to the 4-arm

alternations, we categorize aborted alternations as follows (see Table 4):

6. 3-arm alternations correspond to the consecutive exploration of 3 different arms, followed by the re-entry in the first arm of the sequence, such as $\overrightarrow{A \leftrightarrow B \leftrightarrow C \leftrightarrow A}$.
7. 2/3-arm alternations correspond to the visits of 3 different arms but not in a consecutive manner, such as $\overrightarrow{A \leftrightarrow B \leftrightarrow A \leftrightarrow C}$.
8. 2-arm alternations are the exploration of only 2 arms in a 4-arm sequence, such as $\overrightarrow{A \leftrightarrow B \leftrightarrow A \leftrightarrow B}$.

In contrast mode, 8.5-month-old AD⁺ mice show a significant decrease of 4-arm alternations and concomitant increase of 2/3-arm and 2-arm alternations (Figure 5A) when compared to age-matched WT mice (Genotype \times Sequence, $F_{(3, 69)} = 14.38$, $P < 0.0001$). We further classify aborted alternations (3-arm and 2/3-arm alternations) into pathways of alternations (Figure 4A) as we do for full 4-arm alternations.

9. 3-arm alternations contain sequences from two pathways and correspond to a change of path during exploration.
10. 2/3-arm alternations represent changes of direction within a path.

While AD⁺ mice show a general decrease of all three pathways for 4-arm alternations and increase for 2/3-arm alternations, the change in 3-arm alternations is specific to path \square (Genotype \times Path, $F_{(8, 184)} = 2.770$, $P = 0.0065$). Parallel sets charts show the detailed sequences in path \square of 4-arm and 2/3-arm alternations under contrast mode for 8.5-month-old WT and AD⁺ mice (Figure 5B).

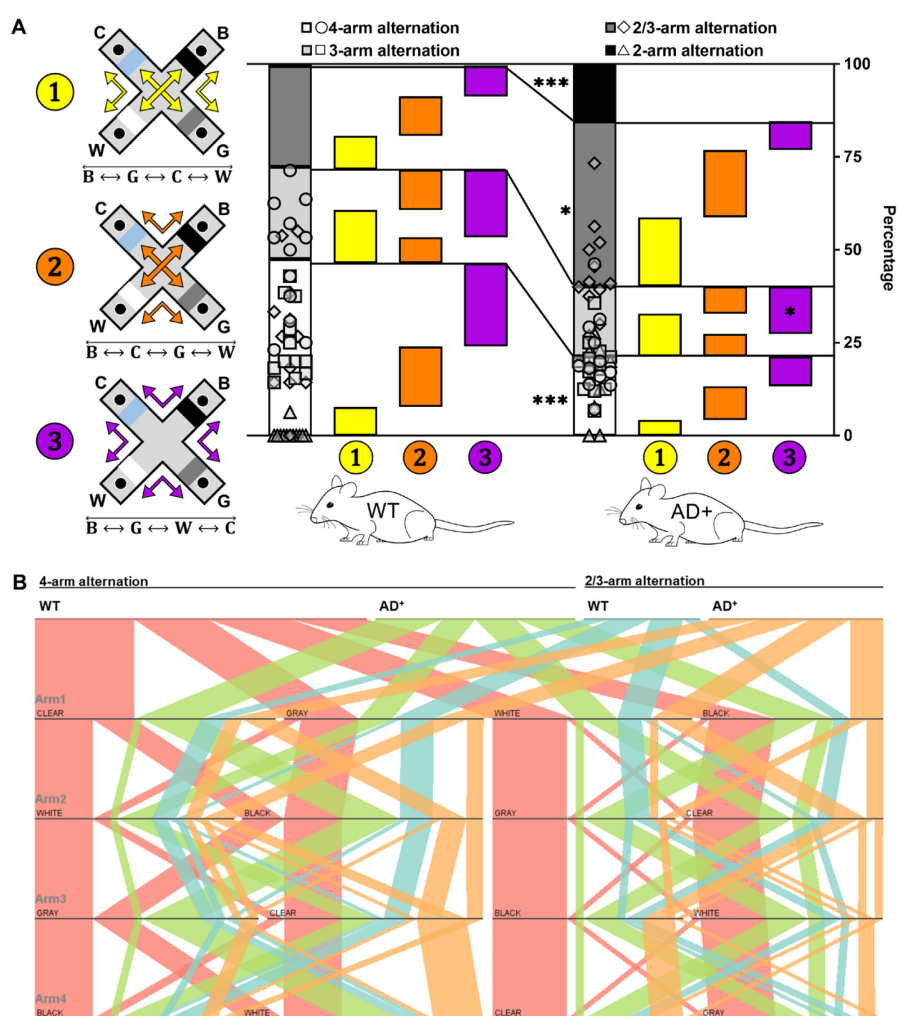


Figure 5. Four-arm sequence analysis in the contrast mode test.

(A) Proportions of the four types of 4-arm sequences and distributions of the three pathways for 8.5-month-old WT and AD⁺ mice in the contrast mode. 4-arm alternations (○), 3-arm alternations (□), 2/3-arm alternations (◊), 2-arm alternations (△). □ $P < 0.05$, □ □ □ $P < 0.001$, WT versus AD⁺ mice. (B) Visualization of 4-arm (WT: red ribbons; AD⁺: green ribbons) and 2/3-arm alternations (WT: blue ribbons; AD⁺: orange ribbons) in 8.5-month-old WT and AD⁺ mice in the contrast mode (Path □ $\overline{B \leftrightarrow G \leftrightarrow W \leftrightarrow C}$) using parallel sets charts.

C. Percentages of time and entries in colored arms

Arm preferences are measured as percentages of time and entries in the differently configured arms. As shown in Figure 6A-6C, between RH and E conditions with different irradiance levels, the proportion of arm visits differ in WT mice. Overall, the red arm, seen as a dark area, is preferred across all conditions of illumination (Figure 6B-6C and see Vit *et al.*, 2021). The difference between conditions occurs essentially in the exploration of the blue, green, and white arms (Figure 6B-6C). While under RH condition these three arms are visited equally, under E condition, when the intensity of the blue source is dramatically increased, the blue becomes the least visited (Time: Condition ×

Color, $F_{(1.876, 20.63)} = 6.069$, $P = 0.0094$; Entries: Condition \times Color, $F_{(1.730, 52.49)} = 6.826$, $P = 0.0035$). These results further validate that the mice use the lights as cues to navigate the ViS4M.

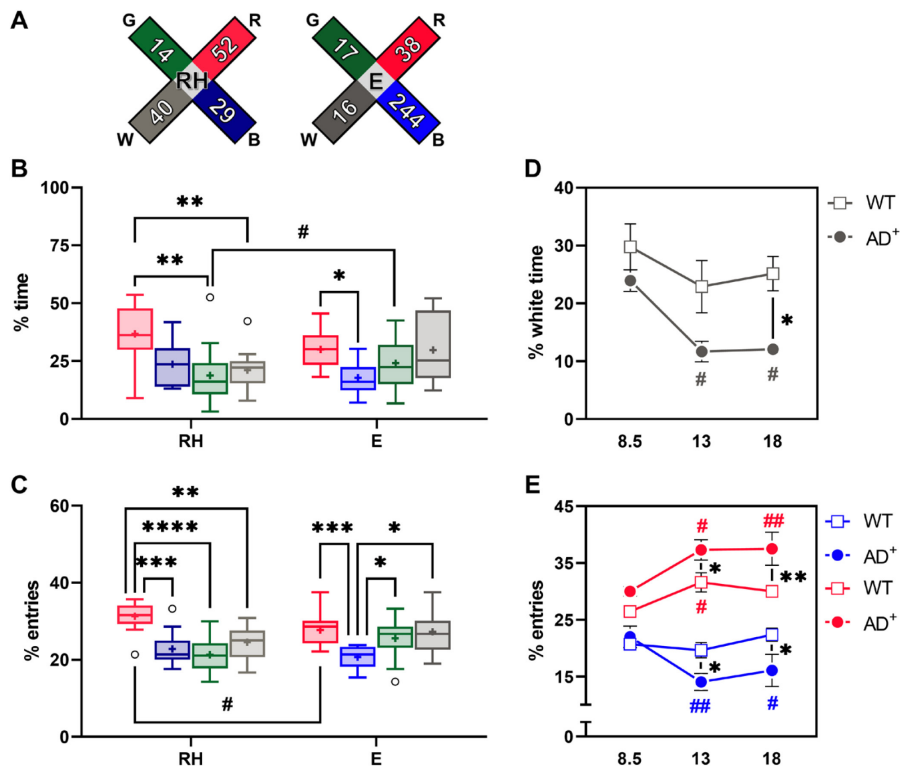


Figure 6. Time and entries in colored arms.

(A) Illustration of the RH and E conditions with measured irradiances in $\mu\text{W}/\text{cm}^2$. (B) Percentages of time spent in each colored arm of young adult (8.5 months) WT mice under RH and E conditions. (C) Percentages of entries in each colored arm of young adult (8.5 months) WT mice under RH and E conditions. (B-C) $\square P < 0.05$, $\square\square P < 0.01$, $\square\square\square P < 0.001$, $\square\square\square\square P < 0.0001$, Red versus Blue versus Green versus White arms; $\# P < 0.05$, RH versus E conditions. (D) Percentages of time spent in the white arm of 8.5-, 13- and 18-month-old WT and AD⁺ mice under E condition. (E) Percentages of entries in the red and blue arms of 8.5-, 13- and 18-month-old WT and AD⁺ mice under E condition. (D-E) $\square P < 0.05$, WT versus AD⁺ mice; $\# P < 0.05$, $\#\#\# P < 0.01$, 8.5 versus 13 and 18 months.

The ViS4M allows the detection of avoidance of both the white and the blue arms by AD⁺ mice under E condition, as shown by the percentage of time spent in the white arm (Genotype, $F_{(1, 67)} = 13.28$, $P = 0.0005$; Age, $F_{(2, 67)} = 5.004$, $P = 0.0094$) and the percentage of entries in the blue arm (Genotype \times Age, $F_{(2, 57)} = 3.541$, $P = 0.0355$) when compared to WT mice (Figure 6D-6E). These results could indicate an age-dependent hypersensitivity of AD⁺ mice to light that is related to its wavelength rather than its absolute irradiance. In humans, AD is associated with both the degeneration of intrinsically photosensitive melanopsin-containing retinal ganglion cells (ipRGCs) and a loss of the pupillary light reflex (PLR), which may give rise to higher light sensitivity.

D. Transitions between arms

Since WT mice tend to alternate between the four arms of the ViS4M in presence of light stimuli, we speculate that transitions between arms could potentially indicate their discrimination between color, light intensity, and/or contrast.

Below are definitions of unidirectional and bidirectional transitions (see example and calculations in Table 3).

1. Unidirectional transitions are defined as the movements from an arm to the following arm in a sequence.
2. From each arm, there are 3 possible destinations, which gives a total of 12 unidirectional transitions.

As presumed from the alternation sequence analysis, the comprehensive study of overall unidirectional transitions highlights visual deficits of AD⁺ mice in discrimination of the white, blue and green light stimuli (Genotype × Transition, $F_{(3, 89)} = 9.469$, $P < 0.0001$) under RH condition (Figure 7). AD⁺ mice are less likely to transition between the blue and white arms in both directions, and between the green and white arms, especially from green to white when compared to WT mice (Figure 7A). However, they favor straight-line transitions between the blue and green arms (Figure 7A), likely reflecting repetitive/impulsive behavior. These results support the preferential use of the path □ of alternation in WT mice and paths □ and □ in AD⁺ mice (Figure 4B-4C).

We use chord diagrams to visualize unidirectional transitions between colored arms. The diagrams are created using the freely available Circos online software. The following rules describe our chord diagrams for unidirectional transitions (Figure 7B):

- a. The segments correspond to and are colored as the four arms of the ViS4M.
- b. The ribbons between segments represent unidirectional transitions and are colored as the originating arm.
- c. Ribbon caps are added at the start to better appreciate their destination.
- d. The most frequent (fourth quartile) and the least frequent (first quartile) transitions are presented on separate diagrams to prevent an overload of ribbons.

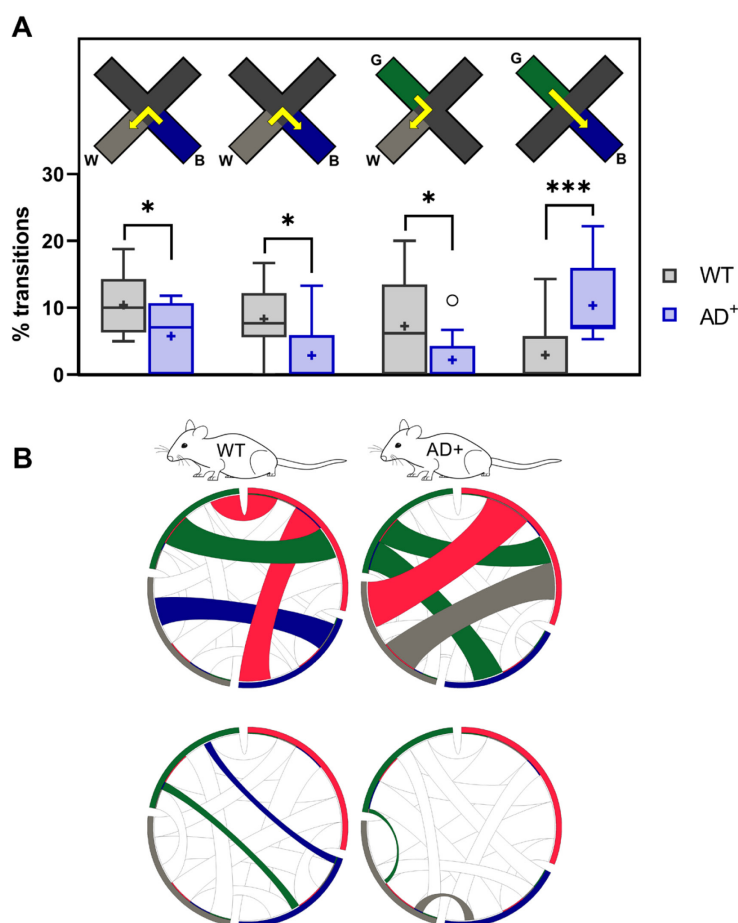


Figure 7. Unidirectional transitions in 8.5-month-old WT and AD⁺ mice under RH condition. (A) Percentages of B→W, W→B, G→W, and G→B transitions. □ $P < 0.05$, □ □ □ $P < 0.001$, WT versus AD⁺ mice. (B) Chord diagrams of the most frequent (top) and least frequent (bottom) unidirectional transitions.

The following pertains to the description of bidirectional transitions.

3. Bidirectional transitions are the transitions between two arms in both directions.
4. The transitions between two arms in both directions do not need to be consecutive to be counted as bidirectional (see red-green transitions in Table 3).
5. There are a total of 6 bidirectional transitions.
6. Bidirectional transitions do not take into account preferences to transition in one particular direction.
7. They are less likely to represent choices based on differences in absolute irradiance.

For bidirectional transitions, all ribbons are color-coded to correspond to the heat-map chart (Figure 8A-8B) as follows:

- a. Black = first quartile (least frequent)
- b. Grey = second quartile
- c. White = third quartile

d. Orange = fourth quartile (most frequent)

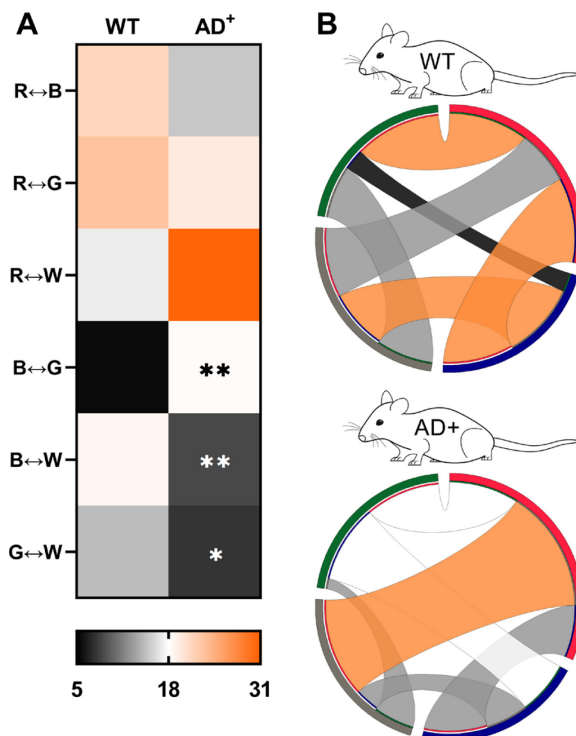


Figure 8. Bidirectional transitions in 8.5-month-old WT and AD⁺ mice under RH condition. (A) Heat map of R↔B, R↔G, R↔W, B↔G, B↔W, and G↔W transitions. □ $P < 0.05$, □ □ $P < 0.01$, WT versus AD⁺ mice. (B) Heat map-coded chord diagrams from the most frequent (orange) to the least frequent (black) bidirectional transitions.

Bidirectional transitions confirm results from alternation sequences and unidirectional transitions analysis. The low percentage of transitions between the blue and green arms in WT mice is expected due to the small difference in irradiance between these two arms (Table 2). It would also mean that WT mice cannot distinguish between the blue and green arms based on chromaticity, which suggests that under the RH condition, the blue light stimulus intensity is below the threshold of activation of the “true” S-cones required for color opponency in mice. However, WT mice are fully able to transition between the blue and white, and green and white arms, with the white arm only slightly brighter than the blue and green arms (the difference of absolute irradiance between the blue and white is even smaller than between the blue and green arms), suggesting that discrimination is likely based on chromaticity, and indicating that the intensity of the white light stimulus is sufficient to activate “true” S-cones as opposed to blue light.

E. Correlations

We use linear regression to determine how closely related alternations and transitions are, which could indicate the contributions of cognition and visual function to the behavior seen in the ViS4M.

As previously shown (Vit *et al.*, 2021), under the RH condition, alternations and green-white transitions are tightly correlated in both 8.5 month-old WT and AD⁺ mice (Figure 9A). In addition, in WT but not AD⁺ mice alternations are inversely proportional to red-white transitions (Figure 9B). This is consistent with the preference of path □ in WT mice and path □ in AD⁺ mice. Here, we demonstrate this by the direct positive relationship of green-white transitions to the paths □ and □ of alternation in AD⁺ and WT mice, respectively (Figure 9C). Moreover, as expected, green-white transition increase correlates with a decrease in path □ in both groups of mice (Figure 9D), indicating the importance of this type of transition, at least under the RH condition of illumination. Interestingly, blue-white transitions did not have any sort of relationship with alternation in AD⁺ mice, showing their limiting effect on color discrimination under RH condition. This is further demonstrated with the parallel sets chart of path □ in 8.5-month-old WT and AD⁺ mice under RH condition (Figure 9E).

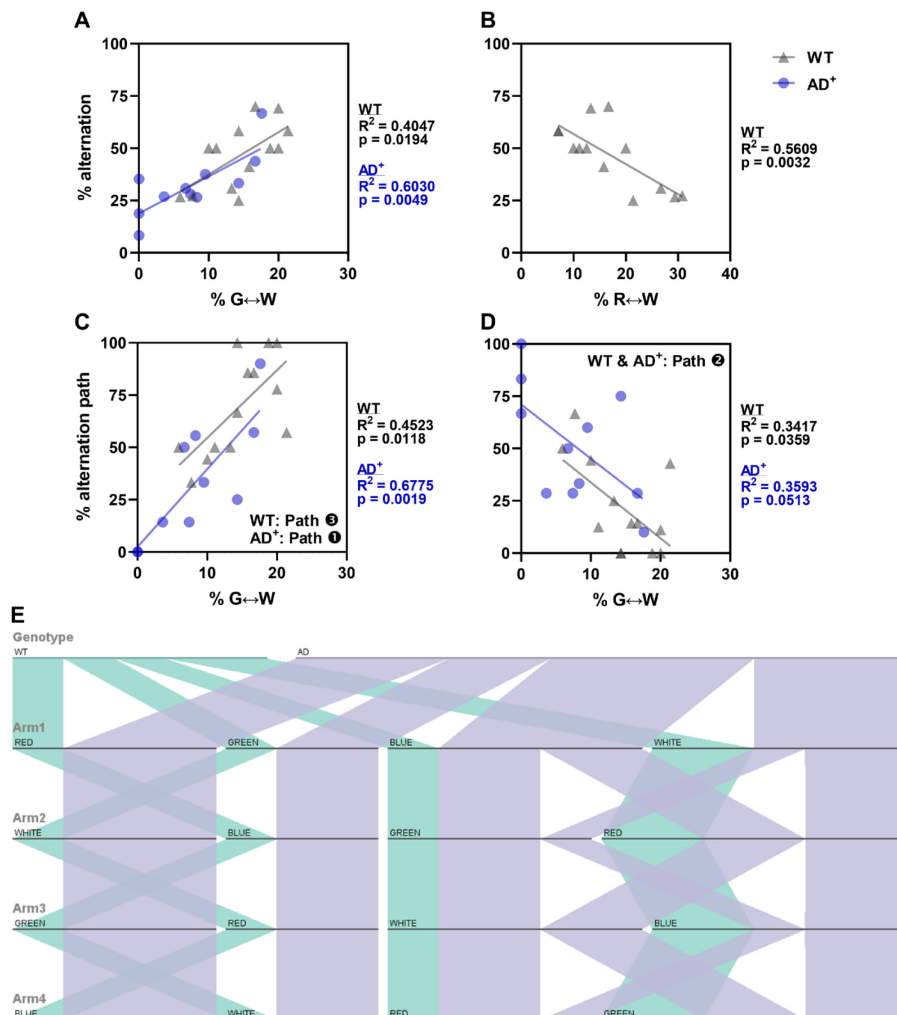


Figure 9. Correlations of alternation performance in 8.5-month-old WT and AD⁺ mice under RH condition.

(A-B) Linear regressions of spontaneous alternation with bidirectional transitions between the

green and white arms (A) or between the red and white arms (B). (C-D) Linear regressions of alternation pathways \square and \square (C), or alternation pathway \square (D) with bidirectional transitions between the green and white arms. (E) Visualization of alternation sequences in 8.5-month-old WT and AD⁺ mice under RH condition (Path \square R \leftrightarrow B \leftrightarrow G \leftrightarrow W) using parallel sets chart.

Notes

In the present manuscript, we sought to provide a detailed but non-exhaustive analysis of our data and share tools that we found helpful to uncover vision deficiencies in AD⁺ mice. We highlight the multi-functionality of the ViS4M. Indeed, we showed that the visual x-maze can be used to measure:

1. Cognitive ability and working memory directly linked to visual function: spontaneous alternation under different conditions of illumination. The ViS4M could offer a great advantage over other cognitive tests that also rely on visual cues and for which locomotor activity can be a bias, such as the Barnes maze. Indeed, in the ViS4M, spontaneous alternation is less likely to be affected by general activity of the animals. In addition, the total number of entries provides an internal control for activity; thus, adding another behavioral test for locomotor activity, such as the open field test, is not necessary.
2. Color and contrast discrimination: arm transitions, alternation sequence analysis. The light stimuli that we chose in our study do not allow us to separate the contribution of S-opsins versus M-opsins. We decided not to use UV lights in our study for obvious safety concerns for the experimenter and the mice. However, future studies may take advantage of the modulatory features of ViS4M and replace blue with UV LEDs, to confirm behavior directly related to S-cone activation and color discrimination. Even though brightness is a confounding factor, our findings support that color (wavelength) discrimination has a key role in mouse visual behavior and in AD⁺ mice deficiency. Although our conditions of illumination can provide a helpful starting point for the design of experiments, the use of the ViS4M is not limited to these settings. We encourage investigators to configure the intensities of the light according to their research goal.
3. Photosensitivity: percentages of time spent/entries in the different arms. We provide evidence that the ViS4M is able to detect simple innate responses to dark (overall preference for the red arm) and bright lights (avoidance of the blue arm). The ViS4M could provide an alternative to the light-dark box test in models of photophobia and anxiety with the possibility to control the brightness of each stimulus.
4. Even though not tested in our study, the ViS4M offers the possibility to pair a light stimulus to an aversive footshock. Thus paradigms of conditioned learning and passive/active avoidance could be imagined using this apparatus.

Overall, the visual-stimuli four-arm maze test, coupled with the analytical tools described here, offers the flexibility to explore multiple behavioral domains in rodents that could be beneficial for the investigation of a wide range of neurological, psychiatric, and ocular conditions.

Acknowledgments

We thank Samuel Fuchs for his original illustration of Figure 1A, Sarah Fuchs for video editing of Supplementary Video 1, and Mia Oviatt for editing the manuscript. The authors dedicate the manuscript to the memories of Dr. Salomon Moni Hamaoui and Lillian Jones Black, who died of Alzheimer's disease.

This manuscript is supported by the National Institute on Aging of the National Institutes of Health under Awards R01 AG055865 and R01 AG056478 (M.K.H.), and The Haim Saban and The Tom Gordon Foundations (M.K.H.). We acknowledge the original research paper where this protocol is derived from: Vit JP, Fuchs DT, Angel A, Levy A, Lamensdorf I, Black KL, Koronyo Y, Koronyo-Hamaoui M. Color and contrast vision in mouse models of aging and Alzheimer's disease using a novel visual-stimuli four-arm maze. *Sci Rep.* 2021 Jan 13;11(1):1255. doi: 10.1038/s41598-021-80988-0. PMID: 33441984; PMCID: PMC7806734 (Vit *et al.*, 2021).

Competing interests

MKH, YK and KLB are co-founders and stockholders of NeuroVision Imaging, Inc., 1395 Garden Highway, Suite 250, Sacramento, CA 95833, USA. MKH, YK and KLB are co-inventors on a patent "Visual stimuli maze test for detecting visual abnormalities in prodromal alzheimer's disease and in alzheimer's disease" application number US16/301,585, filing date 6/2/2017, licensed to Maze Engineers, 5250 Old Orchard Rd., Skokie, Illinois. Ariel Angel, Aharon Levy and Itschak Lamensdorf are former or current employees of Pharmaseed Ltd., Ness Ziona 74047, Israel. Jean-Philippe Vit and Dieu-Trang Fuchs have no competing interests.

Ethics

All experiments followed the NIH Guidelines for the Care and Use of Laboratory Animals and were approved by Cedars-Sinai Medical Center Institutional Animal Care and Use Committee (IACUC protocols 6617 and 8475, valid from February 2016 to February 2022). The study was carried out in compliance with the ARRIVE guidelines.

References

1. Blanks, J. C., Schmidt, S. Y., Torigoe, Y., Porrello, K. V., Hinton, D. R. and Blanks, R. H. (1996a). [Retinal pathology in Alzheimer's disease. II. Regional neuron loss and glial changes in GCL.](#) *Neurobiol Aging* 17(3): 385-395.
2. Blanks, J. C., Torigoe, Y., Hinton, D. R. and Blanks, R. H. (1996b). [Retinal pathology in Alzheimer's disease. I. Ganglion cell loss in foveal/parafoveal retina.](#) *Neurobiol Aging* 17(3): 377-384.

3. Busse, L., Ayaz, A., Dhruv, N. T., Katzner, S., Saleem, A. B., Scholvinck, M. L., Zaharia, A. D. and Carandini, M. (2011). [The detection of visual contrast in the behaving mouse](#). *J Neurosci* 31(31): 11351-11361.
4. Chang, L. Y., Lowe, J., Ardiles, A., Lim, J., Grey, A. C., Robertson, K., Acosta, M. L. (2014). [Alzheimer's disease in the human eye. Clinical tests that identify ocular and visual information processing deficit as biomarkers](#). *Alzheimers Dement* 10(2): 251-261.
5. Chibhabha, F., Yang, Y., Ying, K., Jia, F., Zhang, Q., Ullah, S., Liang, Z., Xie, M. and Li, F. (2020). [Non-invasive optical imaging of retinal Abeta plaques using curcumin loaded polymeric micelles in APPswe/PS1DeltaE9 transgenic mice for the diagnosis of Alzheimer's disease](#). *J Mater Chem B* 8(33): 7438-7452.
6. Chiquita, S., Campos, E. J., Castelhana, J., Ribeiro, M., Sereno, J., Moreira, P. I., Castelo-Branco, M. and Ambrosio, A. F. (2019). [Retinal thinning of inner sub-layers is associated with cortical atrophy in a mouse model of Alzheimer's disease: a longitudinal multimodal in vivo study](#). *Alzheimers Res Ther* 11(1): 90.
7. Criscuolo, C., Cerri, E., Fabiani, C., Capsoni, S., Cattaneo, A., and Domenici, L. (2018). [The retina as a window to early dysfunctions of Alzheimer's disease following studies with a 5xFAD mouse model](#). *Neurobiol Aging* 67: 181-188.
8. Cronin-Golomb, A., Sugiura, R., Corkin, S. and Growdon, J. H. (1993). [Incomplete achromatopsia in Alzheimer's disease](#). *Neurobiol Aging* 14(5): 471-477.
9. Crow, R. W., Levin, L. B., LaBree, L., Rubin, R. and Feldon, S. E. (2003). [Sweep visual evoked potential evaluation of contrast sensitivity in Alzheimer's dementia](#). *Invest Ophthalmol Vis Sci* 44(2): 875-878.
10. Denman, D. J., Luviano, J. A., Ollerenshaw, D. R., Cross, S., Williams, D., Buice, M. A., Olsen, S. R. and Reid, R. C. (2018). [Mouse color and wavelength-specific luminance contrast sensitivity are non-uniform across visual space](#). *Elife* 7: e31209.
11. Doustar, J., Rentsendorj, A., Torbati, T., Regis, G. C., Fuchs, D. T., Sheyn, J., Koronyo-Hamaoui, M. (2020). [Parallels between retinal and brain pathology and response to immunotherapy in old, late-stage Alzheimer's disease mouse models](#). *Aging Cell* 19(11): e13246.
12. Doustar, J., Torbati, T., Black, K. L., Koronyo, Y. and Koronyo-Hamaoui, M. (2017). [Optical Coherence Tomography in Alzheimer's Disease and Other Neurodegenerative Diseases](#). *Front Neurol* 8: 701.
13. Dumitrescu, O. M., Lyden, P. D., Torbati, T., Sheyn, J., Sherzai, A., Sherzai, D., Sherman, D. S., Rosenberry, R., Cheng, S., Johnson, K. O., et al. (2020). [Sectoral segmentation of retinal amyloid imaging in subjects with cognitive decline](#). *Alzheimers Dement (Amst)* 12(1): e12109.
14. Dumitrescu, O. M., Rosenberry, R., Sherman, D. S., Khansari, M. M., Sheyn, J., Torbati, T., Sherzai, A., Sherzai, D., Johnson, K. O., Czeszynski, A. D., et al. (2021). [Retinal venular tortuosity jointly with retinal amyloid burden correlates with verbal memory loss: a pilot study](#). *Cells* 10 (11): 2926.
15. Georgevsky, D., Retsas, S., Raoufi, N., Shimoni, O. and Golzan, S. M. (2019). [A longitudinal](#)

- [assessment of retinal function and structure in the APP/PS1 transgenic mouse model of Alzheimer's disease](#). *Transl Neurodegener* 8: 30.
16. Grimaldi, A., Brighi, C., Peruzzi, G., Ragozzino, D., Bonanni, V., Limatola, C., Ruocco, G. and Di Angelantonio, S. (2018). [Inflammation, neurodegeneration and protein aggregation in the retina as ocular biomarkers for Alzheimer's disease in the 3xTg-AD mouse model](#). *Cell Death Dis* 9(6): 685.
 17. Habiba, U., Merlin, S., Lim, J. K. H., Wong, V. H. Y., Nguyen, C. T. O., Morley, J. W., Bui, B. V. and Tayebi, M. (2020). [Age-Specific Retinal and Cerebral Immunodetection of Amyloid-beta Plaques and Oligomers in a Rodent Model of Alzheimer's Disease](#). *J Alzheimers Dis* 76(3): 1135-1150.
 18. Hampel, H., Toschi, N., Babiloni, C., Baldacci, F., Black, K. L., Bokde, A. L. W., Bun, R. S., Cacciola, F., Cavedo, E., Chiesa, P. A., *et al.* (2018). [Revolution of Alzheimer Precision Neurology. Passageway of Systems Biology and Neurophysiology](#). *J Alzheimers Dis* 64(s1): S47-S105.
 19. Hart, N. J., Koronyo, Y., Black, K. L. and Koronyo-Hamaoui, M. (2016). [Ocular indicators of Alzheimer's: exploring disease in the retina](#). *Acta Neuropathol* 132(6): 767-787.
 20. Jacobs, G. H., Williams, G. A. and Fenwick, J. A. (2004). [Influence of cone pigment coexpression on spectral sensitivity and color vision in the mouse](#). *Vision Res* 44(14): 1615-1622.
 21. Javaid, F. Z., Brenton, J., Guo, L. and Cordeiro, M. F. (2016). [Visual and Ocular Manifestations of Alzheimer's Disease and Their Use as Biomarkers for Diagnosis and Progression](#). *Front Neurol* 7: 55.
 22. Koronyo, Y., Biggs, D., Barron, E., Boyer, D. S., Pearlman, J. A., Au, W. J., Kile, S. J., Blanco, A., Fuchs, D. T., Ashfaq, A., *et al.* (2017). [Retinal amyloid pathology and proof-of-concept imaging trial in Alzheimer's disease](#). *JCI Insight* 2(16): e93621.
 23. Koronyo, Y., Salumbides, B. C., Black, K. L. and Koronyo-Hamaoui, M. (2012). [Alzheimer's disease in the retina: imaging retinal abeta plaques for early diagnosis and therapy assessment](#). *Neurodegener Dis* 10(1-4): 285-293.
 24. Koronyo-Hamaoui, M., Koronyo, Y., Ljubimov, A. V., Miller, C. A., Ko, M. K., Black, K. L., Schwartz, M. and Farkas, D. L. (2011). [Identification of amyloid plaques in retinas from Alzheimer's patients and noninvasive in vivo optical imaging of retinal plaques in a mouse model](#). *Neuroimage* 54 Suppl 1: S204-217.
 25. Kraeuter, A. K., Guest, P. C. and Sarnyai, Z. (2019). [The Y-Maze for Assessment of Spatial Working and Reference Memory in Mice](#). *Methods Mol Biol* 1916: 105-111.
 26. La Morgia, C., Ross-Cisneros, F. N., Koronyo, Y., Hannibal, J., Gallassi, R., Cantalupo, G., Sambati, L., Pan, B. X., Tozer, K. R., Barboni, P., *et al.* (2016). [Melanopsin retinal ganglion cell loss in Alzheimer disease](#). *Ann Neurol* 79(1): 90-109.
 27. Lee, S., Jiang, K., McIlmoyle, B., To, E., Xu, Q. A., Hirsch-Reinshagen, V., Mackenzie, I. R., Hsiung, G. R., Eadie, B. D., Sarunic, M. V., Beg, M. F., Cui, J. Z. and Matsubara, J. A. (2020).

- [Amyloid Beta Immunoreactivity in the Retinal Ganglion Cell Layer of the Alzheimer's Eye.](#) *Front Neurosci* 14: 758.
28. Lemmens, S., Van Craenendonck, T., Van Eijgen, J., De Groef, L., Bruffaerts, R., de Jesus, D. A., Charle, W., Jayapala, M., Sunaric-Megevand, G., Standaert, A., et al. (2020). [Combination of snapshot hyperspectral retinal imaging and optical coherence tomography to identify Alzheimer's disease patients.](#) *Alzheimers Res Ther* 12(1): 144.
29. Mirzaei, M., Pushpitha, K., Deng, L., Chitranshi, N., Gupta, V., Rajput, R., Mangani, A. B., Dheer, Y., Godinez, A., McKay, M. J., et al. (2019). [Upregulation of Proteolytic Pathways and Altered Protein Biosynthesis Underlie Retinal Pathology in a Mouse Model of Alzheimer's Disease.](#) *Mol Neurobiol* 56(9): 6017-6034.
30. Ngolab, J., Donohue, M., Belsh, A., Salazar, J., Cohen, P., Jaiswal, S., Tan, V., Gesser, D., Korouri, S., Aggarwal, N. T., et al. (2021). [Feasibility study for detection of retinal amyloid in clinical trials: the anti-amyloid treatment in asymptomatic Alzheimer's disease \(A4\) trial.](#) *Alzheimers Dement (Amst)*. 13 (1): e12199.
31. Ning, A., Cui, J., To, E., Ashe, K. H. and Matsubara, J. (2008). [Amyloid-beta deposits lead to retinal degeneration in a mouse model of Alzheimer disease.](#) *Invest Ophthalmol Vis Sci* 49(11): 5136-5143.
32. Perez, S. E., Lumayag, S., Kovacs, B., Mufson, E. J. and Xu, S. (2009). [Beta-amyloid deposition and functional impairment in the retina of the APPswe/PS1DeltaE9 transgenic mouse model of Alzheimer's disease.](#) *Invest Ophthalmol Vis Sci* 50(2): 793-800.
33. Polo, V., Rodrigo, M. J., Garcia-Martin, E., Otin, S., Larrosa, J. M., Fuertes, M. I., Bambo, M. P., Pablo, L. E. and Satue, M. (2017). [Visual dysfunction and its correlation with retinal changes in patients with Alzheimer's disease.](#) *Eye (Lond)* 31(7): 1034-1041.
34. Prusky, G. T. and Douglas, R. M. (2004). [Characterization of mouse cortical spatial vision.](#) *Vision Res* 44(28): 3411-3418.
35. Prusky, G. T., Alam, N. M., Beekman, S. and Douglas, R. M. (2004). [Rapid quantification of adult and developing mouse spatial vision using a virtual optomotor system.](#) *Invest Ophthalmol Vis Sci* 45(12): 4611-4616.
36. Risacher, S. L., Wudunn, D., Pepin, S. M., MaGee, T. R., McDonald, B. C., Flashman, L. A., Wishart, H. A., Pixley, H. S., Rabin, L. A., Pare, N., et al. (2013). [Visual contrast sensitivity in Alzheimer's disease, mild cognitive impairment, and older adults with cognitive complaints.](#) *Neurobiol Aging* 34(4): 1133-1144.
37. Risacher, S., WuDunn, D., Tallman, E. F., West, J. D., Gao, S., Farlow, M. R., Brosh, J. R., Apostolova, L. G., Saykin, A. J. (2020). [Visual contrast sensitivity is associated with the presence of cerebral amyloid and tau deposition.](#) *Brain Commun* 2(1): fcaa019.
38. Salobarra-García, E., de Hoz, R., Ramirez, A. I., Lopez-Cuenca, I., Rojas, P., Vazirani, R., Amarante, C., Yubero, R., Gil, P., Pinazo-Duran, M. D., et al. (2019). [Changes in visual function and retinal structure in the progression of Alzheimer's disease.](#) *PLoS One* 14(8): e0220535.
39. Shi, H., Koronyo, Y., Fuchs, D. T., Sheyn, J., Wawrowsky, K., Lahiri, S., Black, K. L. and

- Koronyo-Hamaoui, M. (2020a). [Retinal capillary degeneration and blood-retinal barrier disruption in murine models of Alzheimer's disease](#). *Acta Neuropathol Commun* 8(1): 202.
40. Shi, H., Koronyo, Y., Rentsendorj, A., Fuchs, D. T., Sheyn, J., Black, K. L., Mirzaei, N. and Koronyo-Hamaoui, M. (2021). [Retinal vasculopathy in Alzheimer's disease](#). *Front Neurosci*. 15: 731614.
41. Shi, H., Koronyo, Y., Rentsendorj, A., Regis, G. C., Sheyn, J., Fuchs, D. T., Kramerov, A. A., Ljubimov, A. V., Dumitrascu, O. M., Rodriguez, A. R., *et al.* (2020b). [Identification of early pericyte loss and vascular amyloidosis in Alzheimer's disease retina](#). *Acta Neuropathol* 139(5): 813-836.
42. Sinex, D. G., Burdette, L. J. and Pearlman, A. L. (1979). [A psychophysical investigation of spatial vision in the normal and reeler mutant mouse](#). *Vision Res* 19(8): 853-857.
43. Tadokoro, K., Yamashita, T., Kimura, S., Nomura, E., Ohta, Y., Omote, Y., Takemoto, M., Hishikawa, N., Morihara, R., Morizane, Y. *et al.* (2021). [Retinal amyloid imaging for screening Alzheimer's disease](#). *J Alzheimers Dis* 83 (2): 927-934.
44. van Alphen, B., Winkelman, B. H. and Frens, M. A. (2009). [Age- and sex-related differences in contrast sensitivity in C57BL/6 mice](#). *Invest Ophthalmol Vis Sci* 50(5): 2451-2458.
45. Vit, J. P., Fuchs, D. T., Angel, A., Levy, A., Lamensdorf, I., Black, K. L., Koronyo, Y. and Koronyo-Hamaoui, M. (2021). [Color and contrast vision in mouse models of aging and Alzheimer's disease using a novel visual-stimuli four-arm maze](#). *Sci Rep* 11(1): 1255.
46. Wijk, H., Berg, S., Sivik, L. and Steen, B. (1999). [Colour discrimination, colour naming and colour preferences among individuals with Alzheimer's disease](#). *Int J Geriatr Psychiatry* 14(12): 1000-1005.